Journal of Solid State Chemistry 302 (2021) 122358

Contents lists available at ScienceDirect

Journal of Solid State Chemistry

journal homepage: www.elsevier.com/locate/jssc

New efficient lighting device. Part 1. hybrid materials based on inorganic aerogel and metal-organic phosphor

Artem Lebedev [a], Ekaterina Suslova [a], Kristina Runina [a], Andrew Khomyakov [a], Marina Zykova [a], Olga Petrova [a], Roman Avetisov [a], Denis Shepel [b,c], Artyom Astafiev [b], Natalia Menshutina [a], Igor Avetissov [a,*]

[a] Mendeleev University of Chemical Technology of Russia, Moscow, Russia
[b] N.N. Semenov Federal Research Center for Chemical Physics, RAS, Moscow, Russia
[c] Technoinfo LTD, London, UK

ARTICLE INFO

Keywords:
Organic-inorganic hybrid
Silica aerogel
Metal-organic phosphor
Luminescence

ABSTRACT

A novel luminescent organic-inorganic hybrid material "*LightSil*" (hereinafter referred to as HM-LS) has been fabricated. Tris (8-hydroxyquinolate)aluminum (Alq_3) purified by vacuum sublimation to 99.999 wt% was used as an organic phosphor. Silica aerogel was used as an inorganic matrix. Alq_3 intercalation into aerogel structure did not strongly influence on the HM-LS morphology characteristics comparing with the pure aerogel, which indicated that the intercalation had proceed on the molecular level. An aerogel based hybrid was supercritical dried in a carbon dioxide environment under a pressure of 120 bar, at 40 °C at a carbon dioxide consumption of 500 g/h. The synthesis conditions (TEOS:2-propanol ratio) has been optimized to make the HM-LS sample with the best photoluminescence (PL) characteristics. Analysis of the PL spectra showed that the PL peak maximum of HM-LS shifted to longer wavelengths, and the HM-LS spectrum itself broadened by 64%: $FWHM_{Alq3} = 73$ nm, $FWHM_{HM\text{-}LS} = 113 \pm 3$ nm relative to Alq_3 powder PL spectrum. The latter indicated on a change in the electronic structure of Alq_3 in HM-LS in comparison with the nominally pure Alq_3 and this proved the formation of a new hybrid material.

1. Introduction

The problem of the efficiency of light sources is one of the most pressing in energy-saving technologies for home lighting [1,2]. To date, inorganic LED technology of flat lighting devices has become the most widespread and successfully competing with CRT and OLED technologies [3]. Household LED devices have already achieved an energy efficiency of 250–325 lm/W. However, the dot pattern of light emission is one of the serious disadvantages of these devices. Various light-scattering systems are used to create a distributed luminous flux. In general, it reduces the energy efficiency of LED lamps [4].

The search for new highly efficient schemes for lighting devices, along with the search for new luminescent materials, is an urgent task. As a part of our research project, we consistently tried to solve the problems associated with the creation of a new luminescent material and the creation of a new effective lighting device scheme.

The general idea of the effective lighting device scheme is not new. It includes UV LED lighting system with a phosphor converting UV light into white inside a light-scattering matrix. The similar basic scheme for modern LED systems include a blue LED, a semi-transparent film with a phosphor converting blue light into yellow, which by mixing with blue results to white, and a stand-alone light scattering system enhancing the directional lighting diagram [5,6]. Another similar scheme has been applied successfully to QLED technology by using luminescent quantum dots [6].

A promising candidate for the development of new materials is an aerogel. Aerogel is a solid material with a low density from 0.003 to 0.3 g/cm^3, high specific surface area up to 1500 m^2/g, and mean pore size from 10 to 20 nm [7]. Due to its structural characteristics, an aerogel can be used for superinsulation [8], as catalysts [9], supercapacitors [10], sorbents [11], high effective carrier of active substances, including phosphors, and many others. It is important to note that aerogels can be produced based on precursors of various nature (inorganic substances, polymers, biopolymers), and this greatly expands the application

* Corresponding author.
E-mail addresses: aich@muctr.ru, igor_avetisov@mail.ru (I. Avetissov).

https://doi.org/10.1016/j.jssc.2021.122358
Received 30 March 2021; Received in revised form 5 June 2021; Accepted 14 June 2021
Available online 19 June 2021

possibilities. Nowadays, there are many publications devoted to preparation of materials based on hybrid structures [13], aerogels, and phosphors. Such materials are proposed to be used for high performance luminescent devices [12,14], optoelectronic devices, sensors, catalysts, MRI contrast agents, fluorescent labels and other functional materials [15–18], biosensors [19,20], fluorescence chemosensors with carbon dots [21]. In all cases, important advantages can be achieved by using aerogels, namely, an additional protection of phosphors from environment, translucence of aerogels, possibility of interaction of phosphors with inner aerogels surface.

Our experience in synthesis of organic-inorganic luminescent hybrid materials [22,23] and inorganic silica aerogels [24,25] let's proposed a strategy of a new luminescent hybrid material based on a silica aerogel as an efficient light scattering inorganic matrix with sufficient porous capacity for incorporation of a converting phosphor material. The common light converting phosphors for LED technology are garnet phosphors and similar materials incorporated into stable organic matrix i.e. polyamide, polyacrylamide [26] or polydimethylsiloxane [27]. In spite of the fact that garnet precursors could be made in micro- and nanoscale dimensions by co-precipitation and sol-gel techniques [28] it needs more than 1200 °C heat treatment to synthesized a garnet phosphor [29]. The maximum temperature processing for a silica aerogel fabrication is not more than 50 °C whereas a silica aerogel is degrading when treated at higher than 900 °C [30] or higher than 600 °C [31]. Thus, it is impossible to introduce garnet precursor and conducting phosphor synthesis *in situ* during aerogel fabrication. The similar situation is observed for other inorganic phosphors, which are usually activated at 1000 °C and higher temperatures [32].

Another deal when we have soluble metal-organic and organic electrophosphors [33]. Their technologies have been developed for large scale production of OLED devices. Among the organic electrophosphors the first and more investigated is tris(8-oxyquinoline)aluminum, which also demonstrates high efficient photoluminescence [34].

In the presented research we have tried to fabricate and analyze properties of an organo-inorganic luminescent hybrid material based on the inorganic silica aerogel matrix and the metal-organic phosphor i.e. tris(8-oxyquinoline)aluminum. In future we will use this hybrid as light-scattering luminescent layer in a multilayer flat lighting device.

2. Experimental

2.1. Materials

Tetraethoxysilane (TEOS) (≥99.5%), hydrochloric acid (99.995 wt% 38%), ammonia (99.999 wt% 25%), $Al(NO_3)_3$ (99.95 wt%) were purchased from EKOS-1 Ltd., Russia. Water for synthesis and ICP-MS analysis was purified by an AquaMax-Ultra 370 Series water purification system (Young Lin Instruments, South Korea), mineral acids for ICP-MS analysis were purified by a BSB-939-IR surface sublimation system (Berghof GmbH, Germany). All other solvents and reagents were synthetic grade and purchased form Aldrich and Acros Organics. 8-hydroxyquinoline were purchased from Aldrich and additionally purified by vacuum sublimation to 99.999 wt%.

2.2. Synthesis of aerogel

Silica gel monoliths were prepared using the well-known two-step sol-gel process [35]. As a precursor we used TEOS. 2-propanol was used as a solvent, 0.01 M aqueous hydrochloric acid (HCl) solution as an acid catalyst, and 0.5 M (NH_3) aqueous ammonia solution as a base catalyst. The certain concentration of hydrochloric acid made it possible to obtain a transparent material with a settled specific surface area. The certain concentration of ammonia allowed both to reduce the gelation time and to obtain satisfactory final structural characteristics.

The synthesis of silica gels was carried out in two stages: obtaining of sol and gelation. At the stage of sol preparation, TEOS, 2-propanol and hydrochloric acid solution were mixed for 10 min in a glass covered with a film. After stirring, the sol was kept for 24 h at room temperature to complete the hydrolysis reaction of the precursor. Further, for gelation, the base catalyst of ammonia solution was added to the sol. The resulting mixture was stirring for 2–3 min and poured into cylindrical molds to obtain gel monoliths. The gelation was finished in 5–30 min and the resulting material was kept in the molds for at least 24 h to complete all reaction processes. Then gels were removed from the molds and placed in a fourfold volume of 2-propanol.

Table 1
The molar ratio of initial components for silica gels synthesis.

Silica gel sample notation	TEOS, mole	2-propanol, mole	Water from 0.01 HCl, mole	Water from 0.5 M NH_3, mole
Si–3	1	3	3.6	2.7
Si–5	1	5	3.6	2.7
Si–7	1	7	3.6	2.7
Si–9	1	9	3.6	2.7
Si–11	1	11	3.6	2.7

We have been varing the TEOS: 2-propanol ratio because it drastically effected on the final characteristics of aerogels. The TEOS: 2-propanol ratio determined the concentration of the precursor (TEOS) in the reaction mixture and all the main material properties - density, structural characteristics. Using the ratios presented in Table 1 we synthesized the samples and dried them supercritical using procedure described in section 2.4.

2.3. Metal-organic phosphors synthesis and purification

The synthesis of tris(8-hydroxyquinoline) aluminum was conducted in 2-propanol (pH = 10) at 50 °C and continuous mixing for 1 h. Saturated water solution of 1.63 g of $Al(NO_3)_3$ was added dropwise to a stirred warm solution of 1.90 g of 8-hydroxyquinoline (8-Hq) in 50 ml of 2-propanol, which was followed by the addition of 3 ml of NH_4OH solution until pH = 9. The mixture was maintained for 1 h at constant stirring and heating, and then it was cooled and filtered. The separated precipitate was washed with two portions of *n*-hexane. The obtained material was produced as a light yellow powder. It was purified by vacuum sublimation to 99.9987 wt% measured by ICP-MS analysis (NexION 300D, PerkinElmer Inc.) (see Table S1-S2).

2.4. Synthesis of hybrid material based on silica aerogel and metal-organic phosphors

To produce a hybrid material based on silica aerogel and metal-organic phosphors (HM-LS) the Alq_3 was intercalated into the silica gel before the supercritical drying process by its diffusion from solution into a porous body. The gel was synthesized in 2-propanol, in which the solubility of Alq_3 was limited. Therefore, we replaced the solvent inside the silica gels to acetone, in which the solubility of Alq_3 was higher [22]. To replace the solvent, the synthesized gel (see part 2.2) was put into acetone with continuously shaking for at least 24 h. The volume ratio of gels to acetone was maintained as 1:4. This procedure was repeated three times to minimize the residual content of 2-propanol. Then we placed the

Table 2
The molar ratio of initial components at HM-LS synthesis.

HM-LS sample notation	TEOS, mole	2-propanol, mole	Water from 0.01 HCl, mole	Water from 0.5 M NH_3, mole
Si–3–Alq_3	1	3	3.6	2.7
Si–5–Alq_3	1	5	3.6	2.7
Si–7–Alq_3	1	7	3.6	2.7
Si–9–Alq_3	1	9	3.6	2.7
Si–11–Alq_3	1	11	3.6	2.7

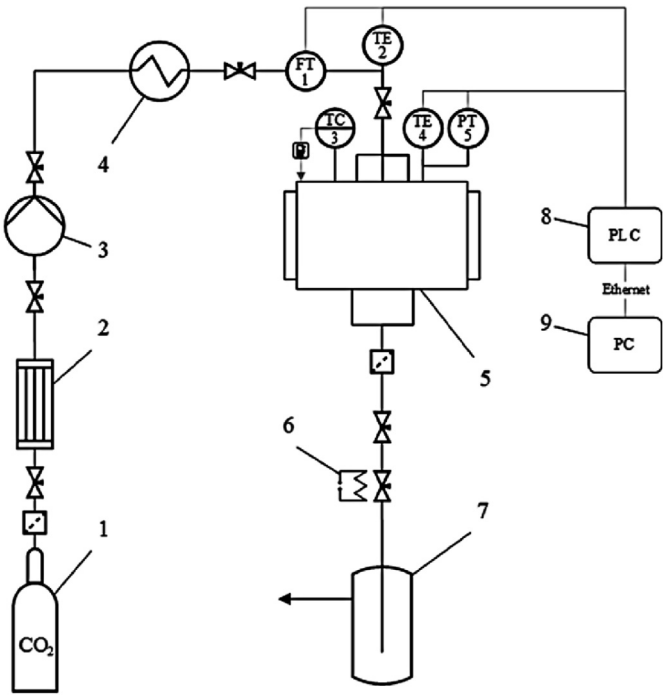

Fig. 1. Scheme of laboratory setup for supercritical drying: 1 – carbon dioxide tank (60 bar); 2 – condenser; 3 – high pressure pump; 4 - heat exchanger; 5 - high-pressure apparatus with 250 ml volume; 6 - heating element; 7 - separator with a cooling jacket; 8 - programmable logic controller (PLC); 9 - personal computer (PC); TC3 - temperature controller; FT1 - Coriolis flowmeter; TE2, TE4 – temperature detectors; PT5 - pressure probe.

gel in a 0.5 wt% solution of Alq_3 in acetone to intercalate Alq_3 into gel pores. The volume ratio of gels to Alq_3 solution was 1:4. To conduct the intercalation procedure the samples were continuously stirring by a shaker for at least 24 h.

We fabricated HM-LS materials with the molar ratios of the initial components similar to the native silica aerogels (Table 2).

To obtain HM-LS we supercritical dried the prepared samples using procedure described in section 2.5. It is important to note that we did not observed noticeable solubility of Alq_3 in supercritical carbon dioxide. Therefore, we assumed the carbon dioxide was an anti-solvent during supercritical drying. Thus, metal-organic phosphors introduced at this stage remained inside the aerogel pores.

2.5. Supercritical drying procedure for aerogel fabrication

The drying process of silica gels and silica gels intercalated by Alq_3 was carried out in a supercritical carbon dioxide medium using a laboratory setup of the original design [36] (Fig. 1).

During the process carbon dioxide flew from tank (1) at 60 bar pressure to condenser (2), where it was cooled down to 298 K to prevent a gas phase formation. A G35 pump (Maximator GmbH, Germany) (3) pressurized the apparatus (5). Before being fed into the apparatus, carbon dioxide was heated in a heat exchanger (4) to reach its supercritical conditions. To control temperature, carbon dioxide mass flow-rate and pressure the setup was equipped with a TE2 thermocouple, a TE4 thermocouple, a FT1 MINI CORI-FLOW™ M13 flow-controller (Bronkhorst, Netherlands) at the inlet of the pressure vessel and a PT5 A-10 pressure probe (WIKA, Germany) inside the pressure vessel. Data from TE2, FT1, TE4, PT5 were fed to a PLC (Production Association Owen Ltd., Russia) (8), and then to a personal computer (9) for processing, monitoring and storage.

Before the start of the process, gels in an organic solvent were placed in a high-pressure apparatus and hermetically sealed. Then carbon dioxide was fed into the apparatus and the process parameters were set as 313 K and 120 bar. The flow-rate of carbon dioxide through the high-pressure apparatus was supported as 500 g/h. The process was carried out for at least 6 h, maintaining the specified parameters. After that, depressurization was carried out at a rate of no more than 4 bar/min. The apparatus was opened and the aerogels were unloaded from the apparatus.

2.6. Analysis of aerogel properties

The fabricated samples were analyzed by different methods to establish the macroscopic and structural characteristics and to reveal their dependence on the synthesis parameters. Aerogels and HM-LS samples were prepared in the form of cylindrical monoliths. The samples' weights in the 1.0–0.1 g range were determined using a PA214C analytical balance (OHAUS Corp., USA) with an accuracy of 0.0001 g. The bulk density (ρ_{bulk}) of silica aerogels and HM-LS were calculated by dividing mass to volume of the cylindrical aerogels. The data standard deviation of the determined ρ_{bulk} did not exceed 0.005 g/cm^3.

The linear shrinkage of the samples was determined as the ratio of the aerogel diameter after drying to the gel diameter after gelation according to the following equation:

$$\boldsymbol{L} = \frac{d_g}{d_a} \cdot 100\%, \quad (1)$$

where d_g – average gel diameter after gelation, m; d_a – average aerogel diameter, m.

The standard deviation for the determined $\boldsymbol{L}$ did not exceed 0.2%.

The structural characteristics of aerogels were studied using low-temperature nitrogen adsorption (77 K) by an ASAP 2020 MP specific surface area and porosity analyzer (Micromeritics Instrument Corp., USA). Before analysis, the samples were degassed at 358 K and <0.5 Torr for 12 h to remove adsorbed moisture. A specific surface area (S_{BET}) was determined by the Brunauer-Emmett-Teller (BET) method. A pore size distribution, mean pore diameter (D) and pore volume (V_{BJH}) were determined by the Barrett-Joyner-Halenda (BJH) method.

An AccuPyc 1340 instrument (Micromeritics Instrument Corp., USA) were used to measure the skeletal density (ρ_{sk}) of materials under study by helium pycnometry. Aerogels' porosity was determined using the bulk and skeletal densities values:

$$\varepsilon = \left(1 - \frac{\rho_{bulk}}{\rho_{sk}}\right) \quad (2)$$

where – ρ_{sk} skeletal density of samples, g/cm^3.

The total pore volume was calculated using the equation:

$$V_{total} = \frac{\varepsilon}{\rho_{sk}} \quad (3)$$

The BJH pore volume (ω) to total pore volume ratio was calculated as following:

$$\omega = \frac{V_{BJH}}{V_{por}} \cdot 100\% \quad (4)$$

Analytical studies were carried out at the Shared Scientific Equipment Center of Mendeleev University.

2.7. SEM and TEM analysis

Micrographs of the samples were recorded on a JEM 2100F high-resolution transmission electronmicroscope (JEOL Co. Ltd., Japan) equipped with a corrector of spherical and chromatic aberration, an energy dispersive X-ray spectral analyzer, and an electron energy loss spectrometer (Gatan, United States), measured at an accelerating voltage of 200 kV. Before measurements, the samples were placed on a copper grid.

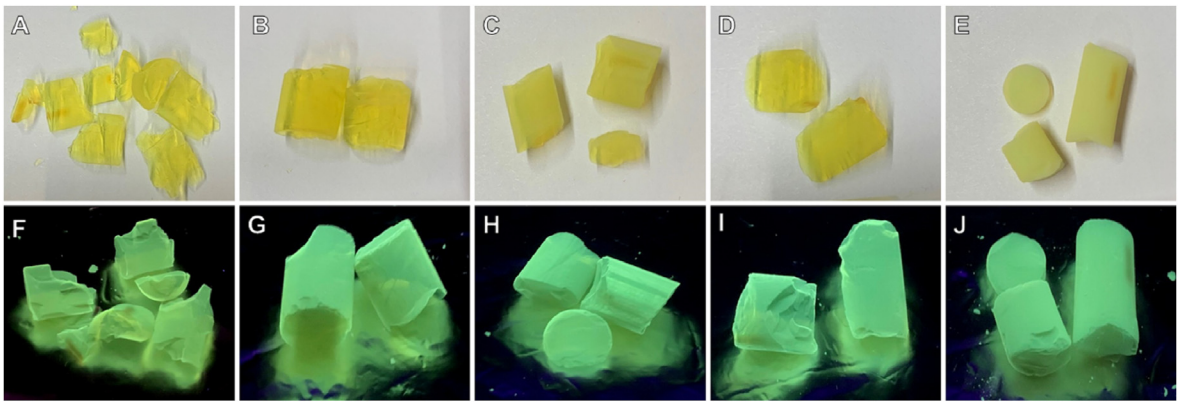

Fig. 2. Photographs of hybrid materials based on silica aerogel and metal-organic phosphors at daylight (upper row) and under UV (365 nm) excitation (bottom row): Si–3–Alq $_3$ (A,F); Si–5–Alq$_3$ (B,G); Si–7–Alq$_3$ (C,H); Si–9–Alq$_3$ (D,I); Si–11–Alq$_3$ (E,J).

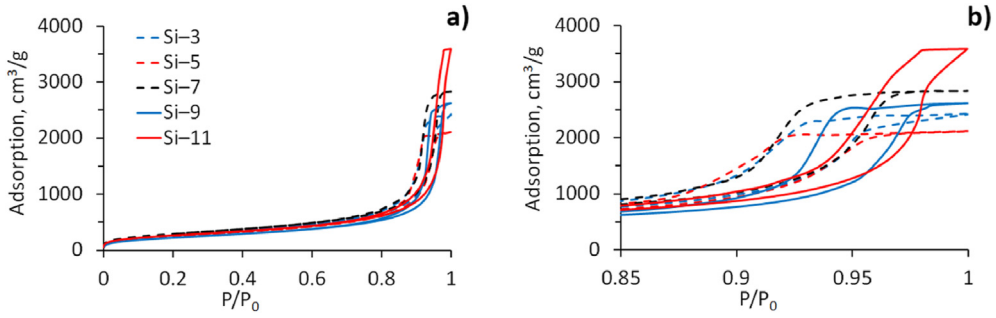

Fig. 3. Nitrogen adsorption/desorption isotherms of silica aerogel samples for P/P_0 range = 0–1.0 (a) and 0.7–1.0 (b).

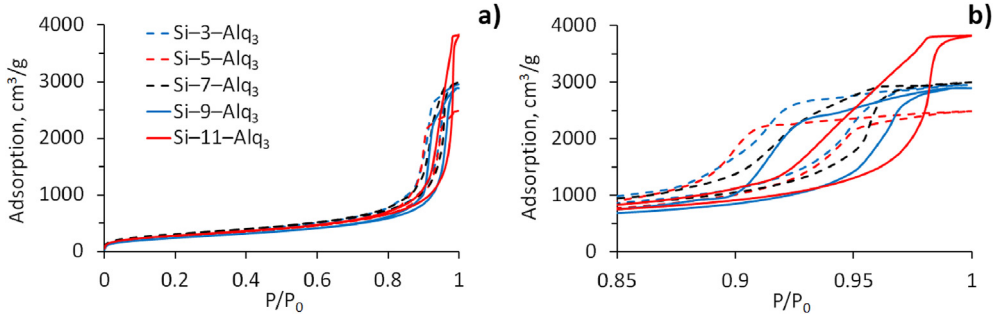

Fig. 4. Nitrogen adsorption/desorption isotherms of HM-LS samples for P/P_0 range: 0–1.0 (a) and 0.85–1.0 (b).

Surface morphology of the samples was analyzed using a JEOL 6510LV scanning electron microscope (JEOL Ltd., Japan). The surface morphology was studied at accelerating voltage from 0.5 to 30 kV. Before measurements, the samples were covered by a conducting layer which was formed by Au vacuum sputtering. Compositional analysis of the films was performed using energy dispersive X-ray (EDX) analysis (INCA Energy 3-D MAX, Oxford Instruments, UK) attached to the SEM.

2.8. Luminescence measurement

All of the luminescence measurements were carried out at room temperature. A Fluorolog FL3-22 spectrofluorimeter (Horiba Jobin Yvon S.A.S., France) with double-grating excitation and emission monochromators was used for luminescence measurements over a wavelength range of 400–800 nm with 0.1 nm step. The luminescence decay kinetics was studied by the excitation of a pulsed diode laser ($\lambda = 377$ nm, $\Delta\tau =$ 1.5 ns) or using a Xenon 450W Ushio UXL-450S/O lamp (355 nm). Processing of the luminescence decay curves was carried out with the OriginPro 8 SR4 software using the Fit Exponential procedure. The final data were averaged over 5 measurements.

3. Results and discussion

All produced HM-LS samples were semi-transparent (Fig. 2 upper row), and their transparency decreased with an increase of 2-propanol concentration at aerogel synthesis. The fabricated HM-LS's demonstrated bright green photoluminescence (PL) under UV excitation (Fig. 2, bottom row).

To determine the structural characteristics, we measured nitrogen adsorption/desorption isotherms (Fig. 3 and Fig. 4).

The isotherms belong to the IV type of adsorption/desorption isotherms according to the IUPAC classification [37]. This type of isotherm is typical for reversible adsorption on mesoporous materials (pore diameter 2–50 nm) by the mechanism of polymolecular adsorption. A characteristic hysteresis loop is observed on the isotherms, since capillary condensation occurs in the mesopores. The hysteresis loops can be

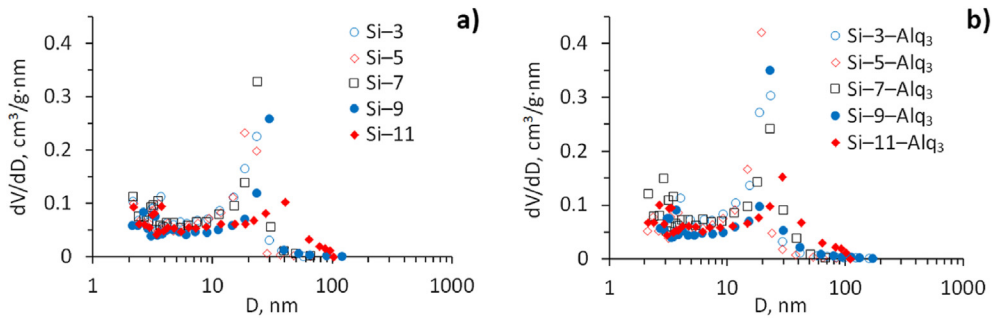

Fig. 5. Pore size distribution of silica aerogels (a) and HM-LS (b).

Table 3
Physical and structural characteristics of silica aerogels and HM-LS.

Sample	ρ_{bulk}, g/cm^3	L, %	S_{BET}, m^2/g	D, nm	V_{BJH}, cm^3/g	ρ_{sk}, g/cm^3	ε	V_{total}, cm^3/g	ω, %	Al/Si, mass ratio
Silica aerogel										
Si–3	0.162	3.9	1017	14.0	3.7	1.90	0.92	5.7	64.9	–
Si–5	0.157	7.2	938	12.9	3.3	1.89	0.92	5.9	55.9	–
Si–7nor	0.114	6.2	1087	15.2	4.4	2.07	0.95	8.3	53.0	–
Si–9	0.095	10.1	839	17.9	4.1	2.24	0.96	10.1	40.6	–
Si–11	0.078	4.1	969	22.2	5.6	2.56	0.97	12.4	45.2	–
HM-LS										
Si–3–Alq$_3$	0.142	7.5	1096	16.8	4.6	1.99	0.93	6.5	70.2	0.011
Si–5–Alq$_3$	0.149	10.8	988	13.8	3.8	1.96	0.92	6.2	61.5	0.010
Si–7–Alq$_3$	0.112	10.0	1121	15.2	4.6	1.98	0.94	8.4	54.8	0.011
Si–9–Alq$_3$	0.111	13.3	907	18.8	4.5	1.89	0.94	8.5	53.1	0.015
Si–11–Alq$_3$	0.082	9.2	1028	21.5	5.9	2.16	0.96	11.7	50.4	0.020

classified as H1 type, which is specific for a porous structure consisting of spherical particles of similar size. With this type of hysteresis loop, the pores in the samples have a shape close to cylindrical. On the basis of the obtained adsorption isotherms, data on the structural characteristics were calculated. Pore size distribution curves for silica aerogel samples (Fig. 5a) and HM-LS samples (Fig. 5b) are plotted.

One can see that the each pore size distribution curve has one distinct peak in the 15–30 nm range and another minor peak at less than 4 nm.

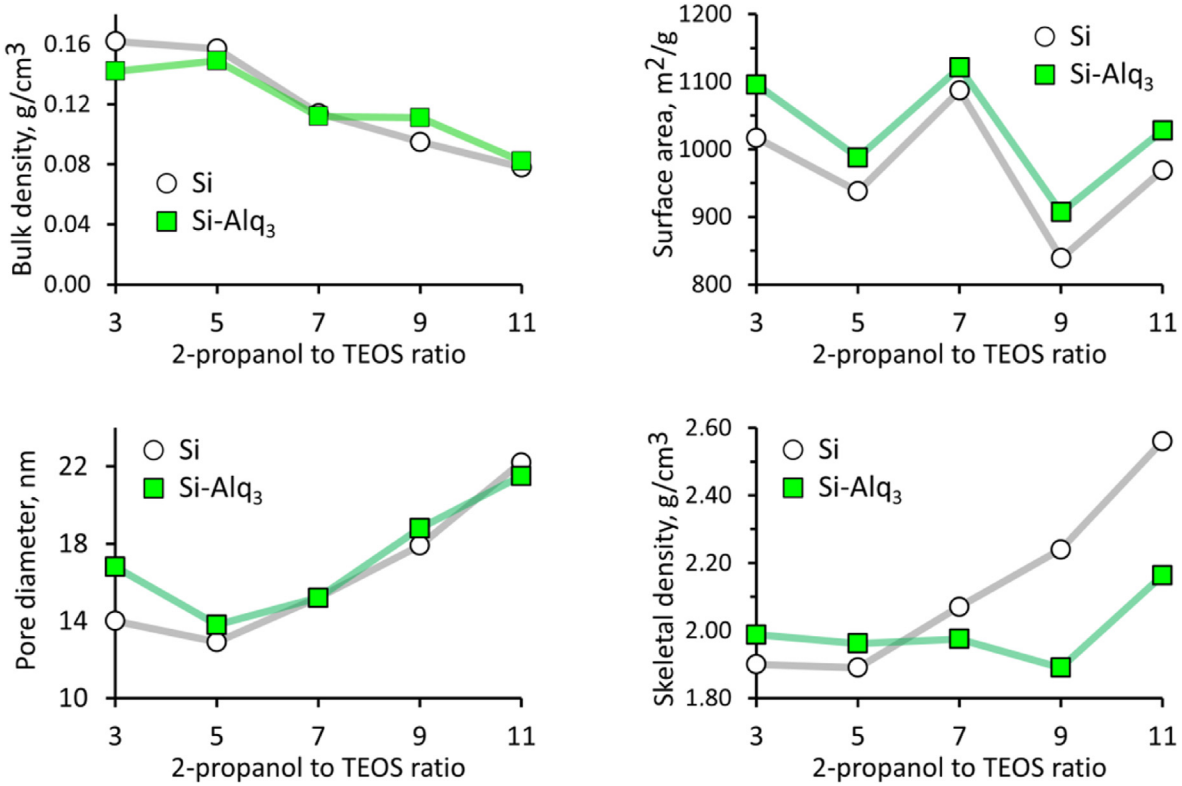

Fig. 6. Bulk density, specific surface area, pore diameter and skeletal density of produced the silica aerogels (Si) and HM-LS (Si–Alq$_3$) at different 2-propanol to TEOS ratios.

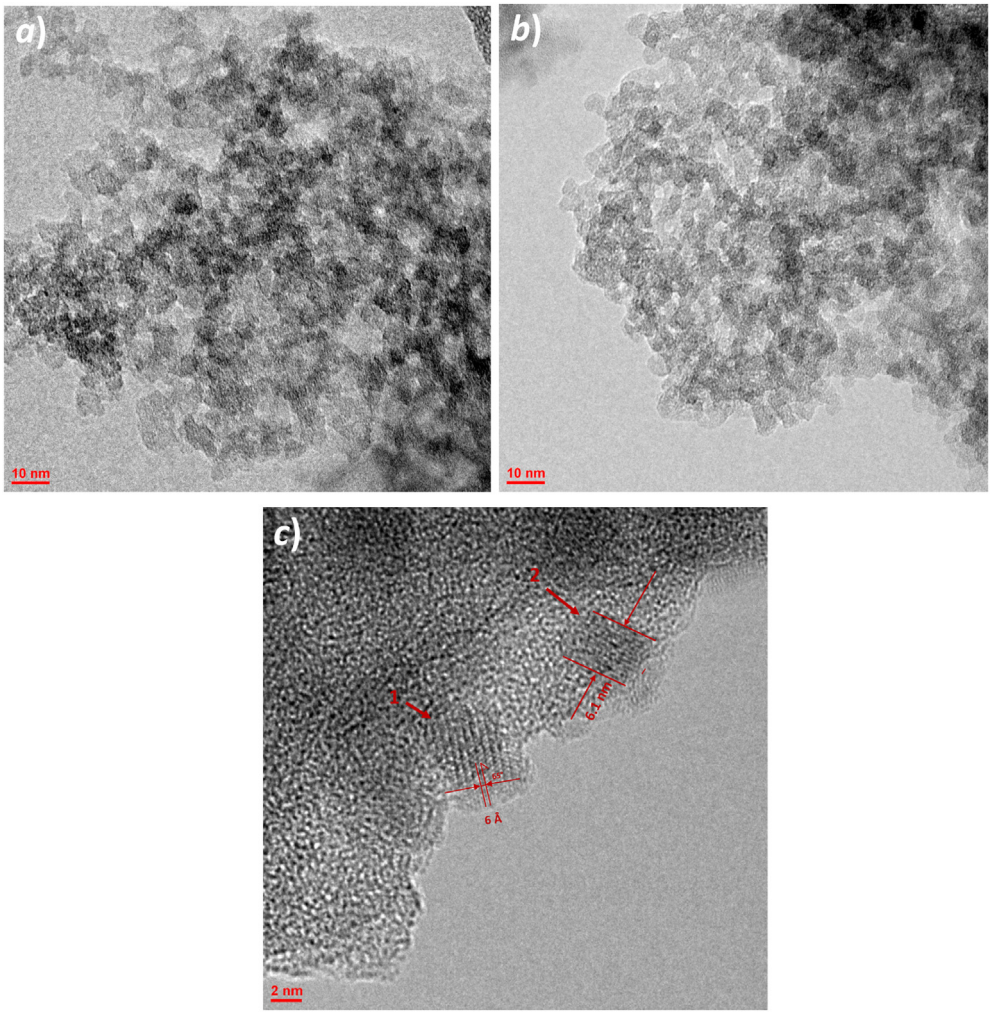

Fig. 7. TEM images of the silica aerogel (*a*) and HM-LS (*b,c*) samples.

The observed peaks indicate that the materials were mesoporous. There is a broadening and shifting of the main peak to the right with 2-propanol content increasing. In the case of Si-5, Si-7, Si-9 samples the shift is small, for Si-3 sample the peak is knocked out of the general trend, and for the Si-11 sample, the shift and broadening of the peak is the most significant. This is probably associated with an increase in the total porosity of the samples with an increase in dilution and generally caused by the features of the sol-gel process.

For nominally pure silica aerogels and HM-LS's we determined: bulk density ρ_{bulk}, shrinkage L, specific surface area S_{BET}, mean pore diameter D, BJH pore volume V_{BJH}, skeletal density ρ_{sk}, porosity ε, total pore volume V_{por} и ratio of BJH pore volume to total pore volume ω (Table 3).

Based on the obtained data, the following patterns can be noted. Shrinkage of the material both without Alq_3 and with Alq_3 was in the range of 3–13% and did not significantly depend on the amount of 2-propanol. In general, shrinkage was greater for HM-LS materials. This is probably due to the fact that before the Alq_3 introduction the solvent was replaced in gels, which could cause a slight additional shrinkage. Besides, with an increase of 2-propanol amount caused the linear decrease of the bulk density of the samples in both cases. This resulted from the fact that an increase of the amount of solvent have led to a decrease in the TEOS concentration in the solution, followed by decreasing in the packing density of structure-forming particles of aerogel. As far as the porosity of the samples was also influenced by the packing density of the structure-forming particles that with an increase in the amount of 2-propanol, the porosity and the total pore volume in the samples had also increased. In addition, one could see that the skeletal density of the materials increased with the amount of 2-propanol.

The ratio (ω, %) between the BJH pore volume and the total pore volume is a very important characteristic. The BJH method is appropriate for pore diameter up to 300 nm. At the same time, from the pore size distribution we could see that the pore size of the tested materials generally did not exceed 60 nm (Fig. 5). The total pore volume measured by the helium pycnometry represented the volume of all pores in the material. Thus, the ratio between meso- and macropores in the final material may be estimated through the ratio (ω, %).

The obtained data showed that the ω-ratio in all samples exceeded 40% and slightly decreased with an increase of 2-propanol amount. It should be stressed that the ω-ratio was higher in the HM-LS samples in contrast to the pure aerogels. This may be due to the fact that intercalation of Alq_3 molecules in an aerogel could cause the formation of additional mesopores.

To carry out a comparative study of the structural characteristics of silica aerogels and HM-LS, the various curves have been plotted (Fig. 6). The most representative dependences are shown in Fig. 6 and rest ones can be found in Supplementary (see Fig. S1 and S2).

We found out that the specific surface area was higher and porosity was generally lower for HM-LS materials comparing with the pure aerogels. This resulted from the peculiarities of the Alq_3 distribution over the aerogel pores. It is clear that Alq_3 reduced the overall porosity by occupying the space inside the already formed aerogel pores. Besides, the intercalated Alq_3 molecules might slightly increase the specific surface area of the material.

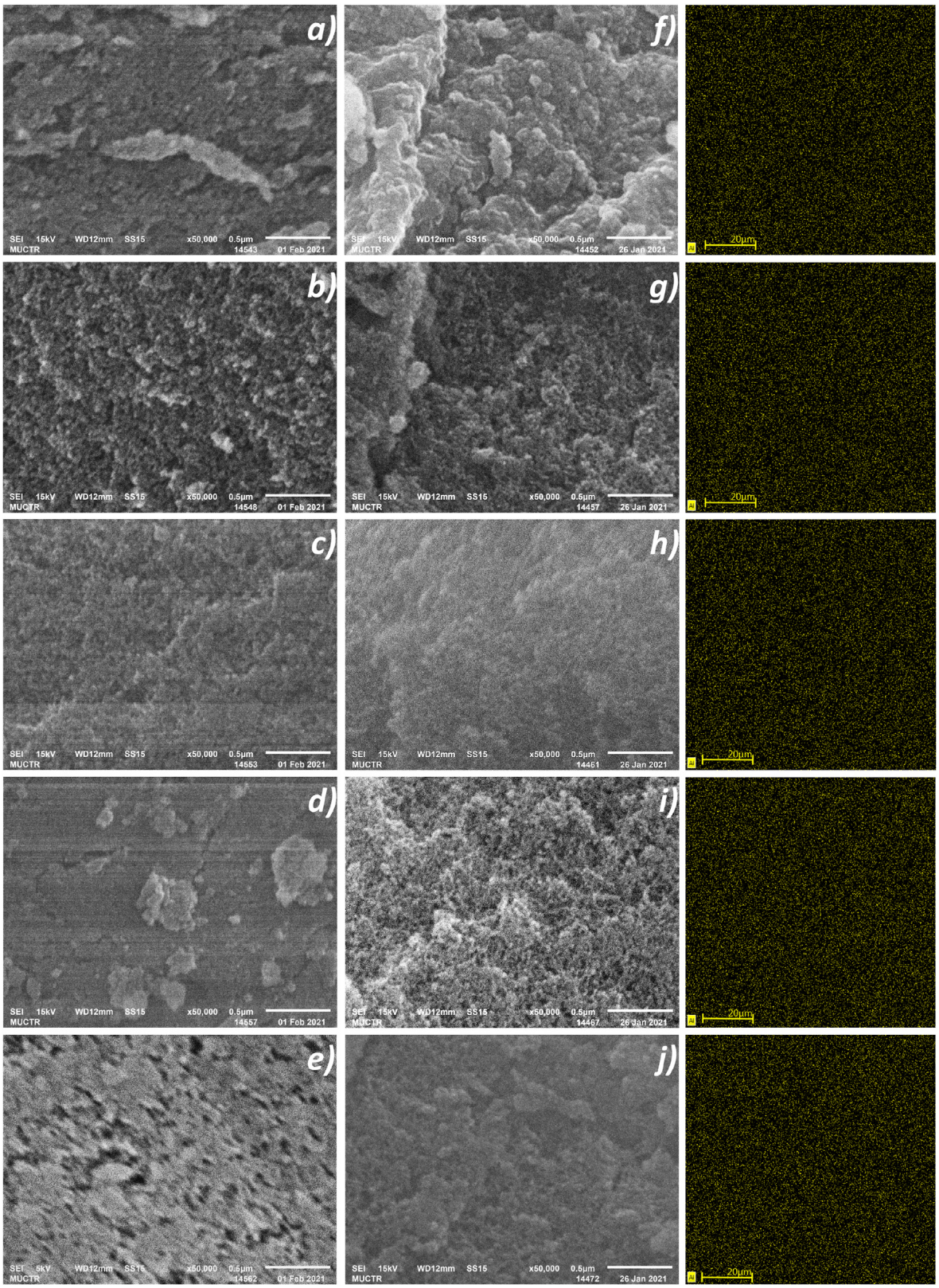

Fig. 8. SEM images of the silica aerogel (left column) and HM-LS (right column) samples: Si–3 (*a*); Si–5 (*b*); Si–7 (*c*); Si–9 (*d*); Si–11 (*e*), Si–3–Alq_3 (*f*); Si–5–Alq_3 (*g*); Si–7–Alq_3 (*h*); Si–9–Alq_3 (*i*); Si–11–Alq_3 (*j*). The right column shows Al mapping of corresponding Si-(i)-Alq_3 samples from EDAX measurements.

The morphology of silica aerogels and HM-LS analyzed by transmission electron microscopy (TEM) (Fig. 7) and scanning electron microscopy (SEM) (Fig. 8) showed that all samples had a developed globular porous structure specific for aerogels.

Nevertheless, in the case of the HM-LS samples we observed local areas with a definite crystalline structure in TEM images (Fig. 7c). The estimated crystalline parameters were about 6 Å and 65°, which were close to α-Alq_3 or δ-Alq_3 [42]. But taking into account the PL maximum

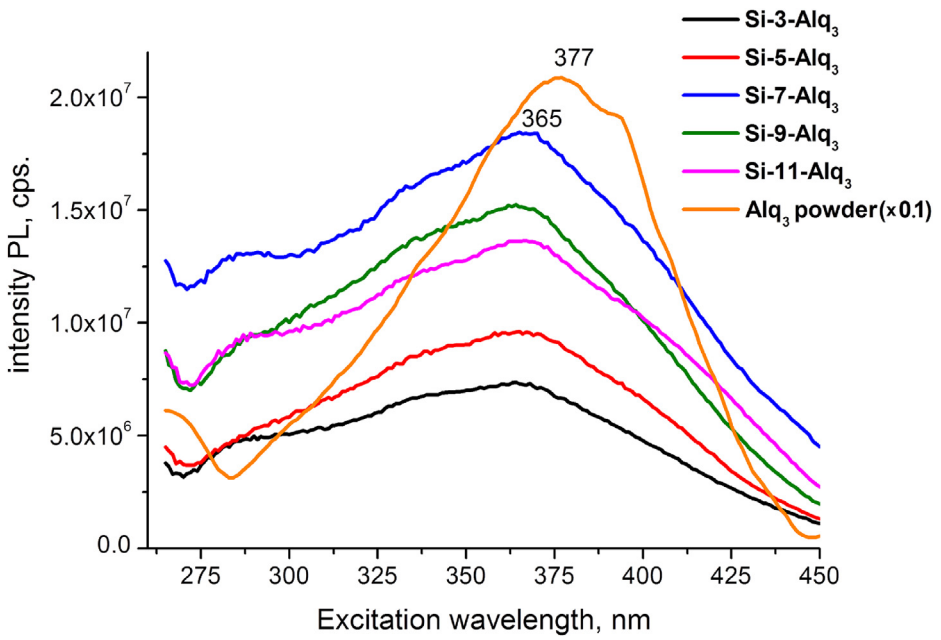

Fig. 9. Excitation spectra of HM-LS samples ($\lambda_{PL} = 521$ nm).

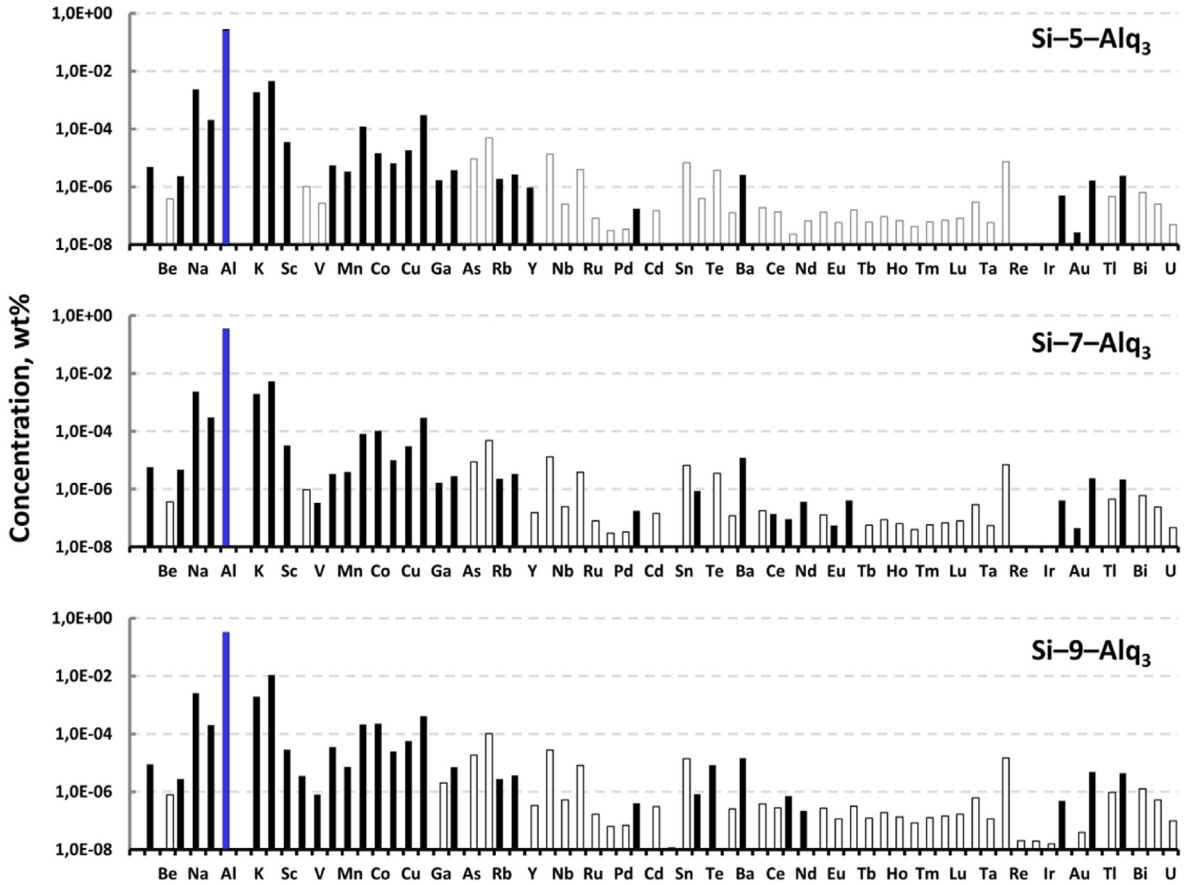

Fig. 10. Impurity content in HM-LS samples. The empty bars indicate the limit of detection (LD) of ICP-MS analysis. The concentrations of the non-presented elements were less 10^{-8} wt%.

$\lambda_{PL}^{max} \approx 521$ nm (Table 4) we assumed that clusters were formed by the α-Alq_3 polymorph because δ-Alq_3 has $\lambda_{PL}^{max} = 481$ nm [34].

According to EDAX analysis Al-based clusters were uniformly distributed in all HM-LS samples (Fig. 8, right column) but the Al-content was different. Taking into consideration a possibility of partial decay of Alq_3 clusters under electron beam radiation, we estimated Al/Si ratio as a parameter, which could characterized Alq_3 intercalation into an aerogel (Table 3, the last right column).

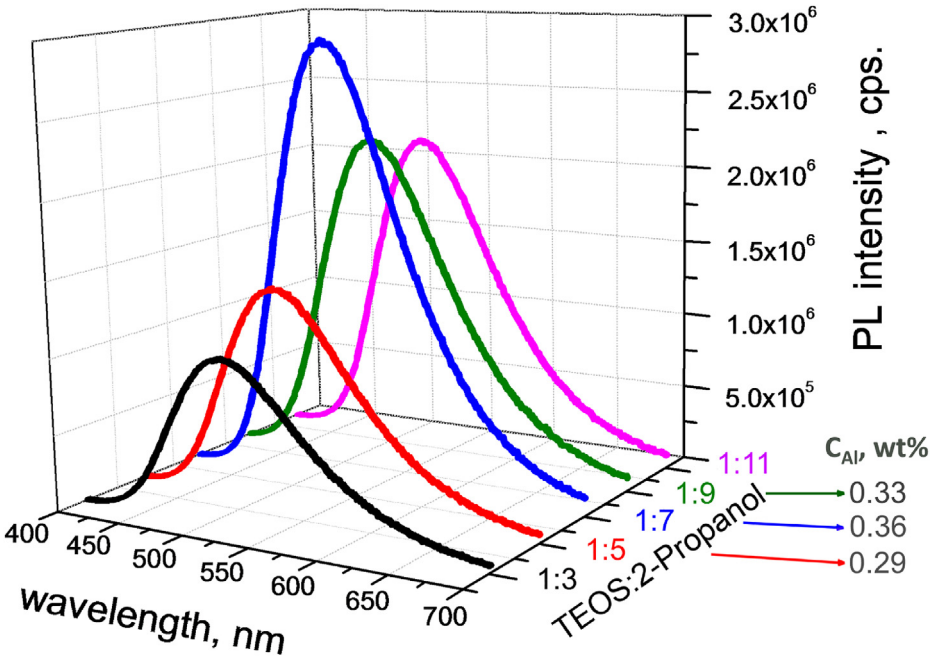

Fig. 11. PL spectra of HM-LS samples (λ_{ext} = 380 nm) and C_{Al} concentration in HM-LS, determined by ICP-MS.

Table 4
PL spectra characteristics of nominally pure Alq_3 powder and HM-LS samples.

HM-LS sample	Area, nm × cps. × 10^{-8}	FWHM, nm	Center, nm	Height, cps. × 10^{-6}	CIE coordinates	
					X	Y
Alq_3 powder	–	73.4	512	–	0.2189	0.5301
Si–3–Alq_3	1.34	114.5	521	1.06	0.2828	0.4608
Si–5–Alq_3	1.76	116.2	521	1.39	0.2769	0.4500
Si–7–Alq_3	3.56	110.8	522	2.92	0.2796	0.4688
Si–9–Alq_3	2.78	115.1	519	2.20	0.2734	0.4455
Si–11–Alq_3	2.58	111.1	524	2.12	0.2851	0.4780

Summarizing the results of morphology analysis, we could conclude that both the silica aerogels and the HM-LS demonstrated a low density from 0.078 to 0.162 g/cm^3, and a high porosity up to 97%. They had a developed specific surface area, consisted of meso- and macropores. The part of mesopores exceeds 40%. Depending on the amount of solvent added at the gel preparation stage we varied the total pore volume in the aerogels from 5.7 to 12.4 cm^3/g.

The excitation spectrum of Alq_3 powder is smooth with a maximum around 380 nm. The excitation spectra of HM-LS's showed a more stretched shape with a maximum 365 nm shifted to the blue region comparing with the Alq_3 powder (Fig. 9). To explain this situation we measured the impurity content in the samples (Fig. 10).

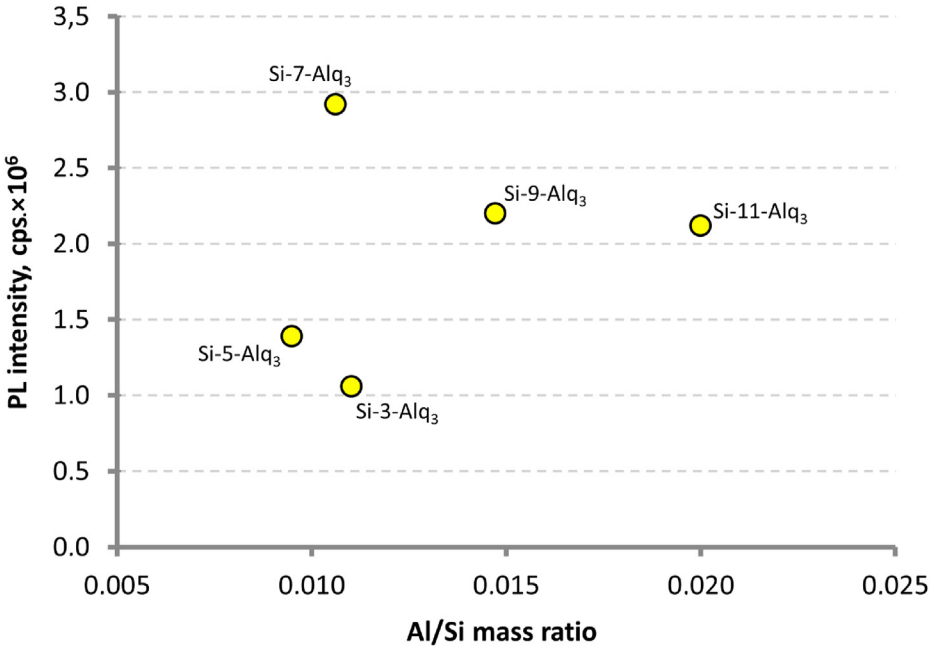

Fig. 12. AL/Si mass ratio *vs* PL intensity of HM-LS samples.

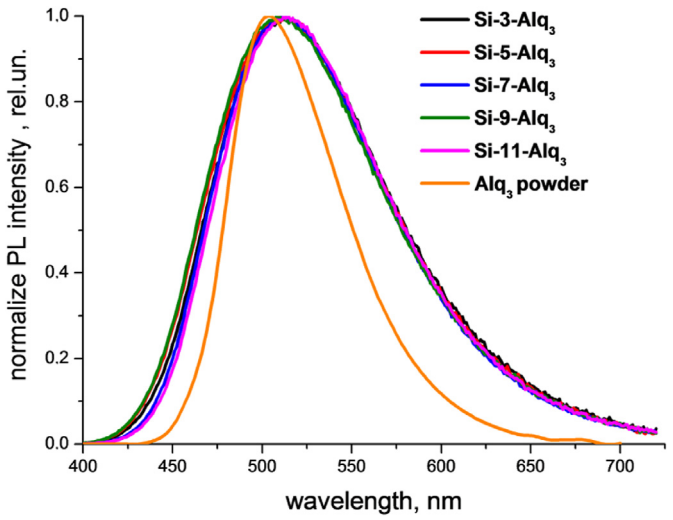

Fig. 13. Normalized PL spectra of nominally pure Alq_3 powder and HM-LS samples.

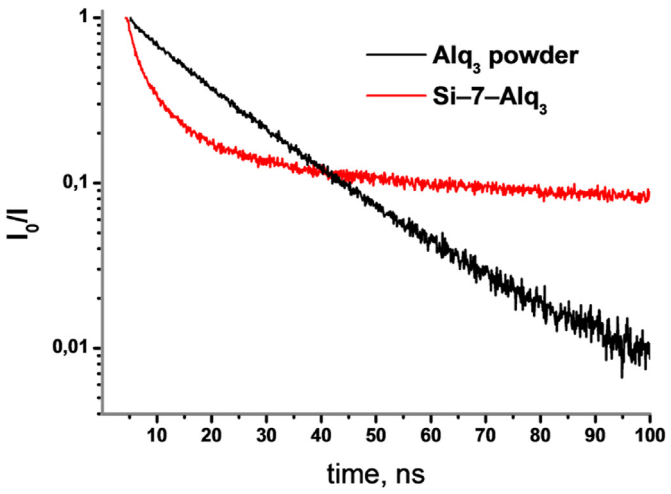

Fig. 14. PL decay kinetics measured at λ_{PL} = 512 nm (Alq_3 powder) and λ_{PL} = 521 nm (Si-7-Alq_3).

Because we introduce Alq_3 into the aerogel the aluminum concentration (the blue bar) was dominant for all the analyzed HL-LS samples (Si-5-Alq_3, Si-7-Alq_3, Si-9-Alq_3) (the precise values are presented in Table S2). One order less contents were measured for Na, K, and Ca. All these metals could form the complexes with 8-Hq, but their PL maximum are shifted to blue spectrum region comparing to Alq_3. Thus, it is hardly possible to explain the nature of the blue shift of the maximum peak at the excitation spectra by the presence of other metal complexes with 8-Hq.

Analysis of the PL emission spectra showed that λ_{PL}^{max} of all HM-LS samples was close to 521 nm. The λ_{PL}^{max} passed through the maximum value at the continuous increase of TEOS:2-propanol ratio (Fig. 11). The PL peak of the Si–7–Alq_3 sample demonstrated record characteristics i.e. the highest PL intensity, the lowest FWHM value and the highest peak area (Table 4).

Comparison of ICP-MS data with PL spectra behavior for HM-LS samples showed that the PL intensity correlated with Al-content in HM-LS samples (see Fig. 11).

Taking in mind that at HM-LS synthesis we added the equal Alq_3 amount to the gel we concluded that the Alq_3 intercalation into the gel synthesized at 1:7 TEOS:2-propanol ratio was more efficient due to the highest value of the specific surface area: 1121 m^2/g for the Si-7-Alq_3 sample and 1087 m^2/g for the Si-7 sample (see Table 3). The comparison of PL intensity with Al/Si mass ratio (Fig. 12) showed that Si-7-Alq_3 sample demonstrated the maximum value of PL intensity at the close values of Al/Si ratio to the Si-3-Alq_3 and Si-5-Alq_3 samples. To explain this result we compare the pore size distribution and structural parameters of the silica aerogels and the HM-LS's (Fig. 5, Table 3). We found out that Si-7 sample had the maximal density of 15 nm pores while for Si-7-Alq_3 this peak significantly reduced. In this case the efficacy of α-Alq_3 intercalation was maximal. For Si-9-Alq_3 and Si-11-Alq_3 samples due to the larger pore size and lower mesopores volume partial washing out of the intercalated Alq_3 could take place. In the case of Si-3-Alq_3 and Si-5-Alq_3 samples the total pore volume was lower and the intercalation of Alq_3 into the aerogel could be suppressed.

The hypothesis of α-Alq_3 intercalation into silica aerogel is also proved by the analysis of PL spectrum behavior. From PL spectra, one can see that λ_{PL}^{max} is close to 521 nm, which is specific for α-, β-, or ε-polymorphs with meridional Alq_3 molecules [38]. Nevertheless, analysis of normalized PL spectra of the nominally pure Alq_3 powder and HM-LS samples (Fig. 13) showed that there was a 10 nm bathochromic shift of λ_{PL}^{max} of HM-LS samples towards Alq_3 powder. There are several reasons, which could explain the bathochromic shift. We assumed that the most probable explanation is related to the compression of Alq_3 molecules in mesopores. It was demonstrated in Ref. [39] that as-grown Alq_3, Gaq_3, Inq_3 crystals containing meridional (mer-) isomer experienced a red shift of nearly 90 nm in the 0–8 GPa range. In our case at the supercritical drying, we used 120 bar CO_2 pressure (only 0.012 GPa). This pressure was enough to shift λ_{PL}^{max} from 512 nm of Alq_3 powder to 521 ± 2 nm of HM-SL samples. The probable compression of Alq_3 molecules in mesopores could also result to the blue shift of the maximum peak at the excitation spectra due to the energy shift of the π*-orbital.

The nominally pure Alq_3 powder had nearly mono-exponential PL decay kinetics with lifetime of 17 ns whereas Si-7-Alq_3 demonstrated two-exponential kinetics (Fig. 14). The fast centers had 3 ns lifetime and the slow centers had 31 ns lifetime (Fig. S3, S4). This correlates with the properties of the bulk HM based on B_2O_3 glass-matrix and organic phosphors Mq_3 (M = Al, Ga, In) [40] for which we had also observed two-exponential kinetics. Thus, the nature of HM-LS and hybrid materials based on inorganic glass matrix of different chemical composition and various organic phosphors [41] is similar in spite of the strong difference in solid density.

We made preliminary experiments to clear up the stability of HM-LS materials. The first samples degraded within several days at room atmosphere. They continuously changed they color from yellow to brown and furthermore dark-brown. The brown samples did not demonstrate any luminescence. Careful washing of the setup for supercritical drying by pure solvents enhanced the HM-LS samples stability. We kept the samples in plastic vessels preliminary blew through and filled by CO_2. Another part of the samples was stored in evacuated quartz ampoules. An exposition of the samples under natural UV lighting during daylight hours and under UV lamp at night during three months reduced PL intensity in 15% for the samples in plastic vessels. In the case of samples kept in the quartz ampoules, we observed just 5% fall of the PL intensity.

4. Conclusions

A novel luminescent organic-inorganic hybrid material "*LightSil*" has been synthesized using tris (8-hydroxyquinolate)aluminum (Alq_3) (99.999 wt%) as an organic phosphor and silica aerogel as an inorganic matrix. An aerogel based hybrid was supercritical dried in a carbon dioxide environment under a pressure of 120 bar, at 40 °C at a carbon dioxide consumption of 500 g/h. The synthesis conditions (TEOS:2-propanol ratio) has been optimized to make the HM-LS sample with the best photoluminescence (PL) characteristics. It was found out that Alq_3 intercalation into aerogel structure did not strongly influence on the HM-LS morphology characteristics comparing with the pure aerogel, which

indicated that the intercalation had proceed on the molecular level. According to the TEM and PL data the intercalated Alq_3 was in the form of α-Alq_3 polymorph associated in 6 nm size clusters.

Analysis of the PL spectra showed that λ_{PL}^{max} of HM-LS shifted to longer wavelengths, and the HM-LS spectrum itself broadened by 64% comparing with Alq_3 powder PL spectrum. The latter indicated on a change in the electronic structure of Alq_3 in HM-LS which could result from the compression of Alq_3 molecules inside the aerogel mesopors.

CRediT authorship contribution statement

Artem Lebedev: Methodology, Formal analysis. **Ekaterina Suslova:** Investigation, Resources. **Kristina Runina:** Investigation. **Andrew Khomyakov:** Data curation. **Marina Zykova:** Writing – review & editing. **Olga Petrova:** Writing – original draft. **Roman Avetisov:** Visualization, Writing – review & editing. **Denis Shepel:** Visualization, Writing – review & editing. **Artyom Astafiev:** Investigation, Writing – review & editing. **Natalia Menshutina:** Supervision, Funding acquisition. **Igor Avetissov:** Validation, Conceptualization.

Declaration of competing interest

The authors declare that they have no known competing financial interests or personal relationships that could have appeared to influence the work reported in this paper.

Acknowledgment

This research was financially supported by the Ministry of Science and Higher Education of Russia, FSSM-2020-0003.

Appendix A. Supplementary data

Supplementary data to this article can be found online at https://doi.org/10.1016/j.jssc.2021.122358.

References

[1] R. Mertens, The Oled Handbook, A Guide to OLED Technology, Industry and Market, Lulu Press, Inc, 2019, 2019.
[2] S. Franky, in: S. Franky (Ed.), Organic Electronics: Materials, Processing, Devices and Applications, Taylor and Francis Group, Boca Raton, 2010.
[3] LED and OLED Lighting: Market Analysis and Manufacturing Trends ID: 5147253 https://www.researchandmarkets.com/reports/5147253/led-and-oled-lighting-market-analysis-and?utm_source=GNOM&utm_medium=PressRelease&utm_code=z6d87v&utm_campaign=1452993+-+Global+LED+and+OLED+Lighting+Market+Analysis+and+Manufacturing+Report+2020%3a+LED+Based+SSL%2c+is+on+Course+to+Become+the+Dominant+Technology+Across+All+Lighting+Applications&utm_exec=chdo54prd.
[4] W.C. Chen, P.H. Liou, B.J. Chen, Optimization design for the dot pattern of led light guide plate using soft computing, J. Appl. Sci. 13 (2013) 2378–2383, https://doi.org/10.3923/jas.2013.2378.2383.
[5] K. Bando, K. Sakano, Y. Noguchi, Y. Shimizu, Development of high-bright and pure-white LED lamps, J. Light Vis. Environ. 22 (1998) 2–5, https://doi.org/10.2150/jlve.22.1_2.
[6] H. Daicho, K. Enomoto, H. Sawa, S. Matsuishi, H. Hosono, Improved color uniformity in white light-emitting diodes using newly developed phosphors, Opt Express 26 (2018), 24784, https://doi.org/10.1364/OE.26.024784.
[7] M.A. Aegerter, N. Leventis, M.M. Koebel (Eds.), Aerogels Handbook, 2011, https://doi.org/10.1007/978-1-4419-7589-8. Springer New York, New York, NY.
[8] M. Koebel, A. Rigacci, P. Achard, Aerogel-based thermal superinsulation: an overview, J. Sol. Gel Sci. Technol. 63 (2012) 315–339, https://doi.org/10.1007/s10971-012-2792-9.
[9] D. Karami, A review of aerogel applications in adsorption and catalysis, J. Pet. Sci. Technol. 8 (2018) 3–15, https://doi.org/10.22078/jpst.2018.3348.1535.
[10] Z. Zhai, B. Ren, Y. Xu, S. Wang, L. Zhang, Z. Liu, Nitrogen self-doped carbon aerogels from chitin for supercapacitors, J. Power Sources 481 (2021), 228976, https://doi.org/10.1016/j.jpowsour.2020.228976.
[11] D. Lovskaya, N. Menshutina, M. Mochalova, A. Nosov, A. Grebenyuk, Chitosan-based aerogel particles as highly effective local hemostatic agents, Production Process and In Vivo Evaluations, Polymers (Basel) 12 (2020), 2055, https://doi.org/10.3390/polym12092055.
[12] H. Wang, Z. Shao, M. Bacher, F. Liebner, T. Rosenau, Fluorescent cellulose aerogels containing covalently immobilized (ZnS)x(CuInS2)1−x/ZnS (core/shell) quantum dots, Cellulose 20 (2013) 3007–3024, https://doi.org/10.1007/s10570-013-0035-z.
[13] L. Xu, V. Selin, A. Zhuk, J.F. Ankner, S.A. Sukhishvili, Molecular weight dependence of polymer chain mobility within multilayer films, ACS Macro Lett. 2 (2013) 865–868, https://doi.org/10.1021/mz400413v.
[14] A. Amlouk, L. El Mir, S. Kraiem, M. Saadoun, S. Alaya, A.C. Pierre, Luminescence of TiO2:Pr nanoparticles incorporated in silica aerogel, Mater. Sci. Eng., B 146 (2008) 74–79, https://doi.org/10.1016/j.mseb.2007.07.056.
[15] W. Zhang, Y. Liu, H. Yu, X. Dong, Eu and Tb co-doped porous SiO2 aerogel composite and its luminescent properties, J. Photochem. Photobiol. Chem. 379 (2019) 47–53, https://doi.org/10.1016/j.jphotochem.2019.04.040.
[16] L. Xu, Z. Chu, H. Wang, L. Cai, Z. Tu, H. Liu, C. Zhu, H. Shi, D. Pan, J. Pan, X. Fei, Electrostatically assembled multilayered films of biopolymer enhanced nanocapsules for on-demand drug release, ACS Appl. Bio Mater. 2 (2019) 3429–3438, https://doi.org/10.1021/acsabm.9b00381.
[17] L. Xu, H. Wang, Z. Chu, L. Cai, H. Shi, C. Zhu, D. Pan, J. Pan, X. Fei, Y. Lei, Temperature-responsive multilayer films of micelle-based composites for controlled release of a third-generation EGFR inhibitor, ACS Appl. Polym. Mater. 2 (2020) 741–750, https://doi.org/10.1021/acsapm.9b01051.
[18] Y. Lu, A. Zhuk, L. Xu, X. Liang, E. Kharlampieva, S.A. Sukhishvili, Tunable pH and temperature response of weak polyelectrolyte brushes: role of hydrogen bonding and monomer hydrophobicity, Soft Matter 9 (2013) 5464, https://doi.org/10.1039/c3sm50268f.
[19] S.W. Allison, E.S. Baker, K.J. Lynch, F. Sabri, In vivo X-Ray excited optical luminescence from phosphor-doped aerogel and Sylgard 184 composites, Radiat. Phys. Chem. 135 (2017) 88–93, https://doi.org/10.1016/j.radphyschem.2017.01.045.
[20] A.B. Solovieva, A.S. Kopylov, M.A. Savko, T.S. Zarkhina, D.D. Lovskaya, A.E. Lebedev, N.V. Menshutina, A.V. Krivandin, I.V. Shershnev, S.L. Kotova, P.S. Timashev, Photocatalytic properties of tetraphenylporphyrins immobilized on calcium alginate aerogels, Sci. Rep. 7 (2017), 12640, https://doi.org/10.1038/s41598-017-12945-9.
[21] Y. Ma, X. Chen, J. Bai, G. Yuan, L. Ren, Highly selective fluorescence chemosensor based on carbon-dot-aerogel for detection of aniline gas, Inorg. Chem. Commun. 100 (2019) 64–69, https://doi.org/10.1016/j.inoche.2018.12.013.
[22] O. Petrova, I. Taydakov, M. Anurova, A. Akkuzina, R. Avetisov, A. Khomyakov, E. Mozhevitina, I. Avetissov, Luminescent hybrid materials based on an europium organic complex and borate glasses, J. Non-Cryst. Solids (2015), https://doi.org/10.1016/j.jnoncrysol.2015.09.012.
[23] O.B. Petrova, M.O. Anurova, A.A. Akkuzina, R.R. Saifutyarov, E.V. Ermolaeva, R.I. Avetisov, A.V. Khomyakov, I.V. Taydakov, I.C. Avetissov, Luminescent hybrid materials based on (8-hydroxyquinoline)-substituted metal-organic complexes and lead-borate glasses, Opt. Mater. (Amst). 69 (2017) 141–147, https://doi.org/10.1016/j.optmat.2017.04.014.
[24] N.V. Men'shutina, A.M. Katalevich, I. Smirnova, Preparation of silica-based aerogels by supercritical drying, Russ. J. Phys. Chem. B. 8 (2014) 973–979, https://doi.org/10.1134/S1990793114070100.
[25] A.E. Lebedev, N.V. Menshutina, I.I. Khudeev, R.A. Kamyshinsky, Investigation of alumina aerogel structural characteristics at different «precursor-water-ethanol» ratio, J. Non-Cryst. Solids 553 (2021), 120475, https://doi.org/10.1016/j.jnoncrysol.2020.120475.
[26] H. Yen Tan, T. Wah Ng, O. Wah Liew, Effects of light spectrum in flatbed scanner densitometry of stained polyacrylamide gels, Biotechniques 42 (2007) 474–478, https://doi.org/10.2144/000112402.
[27] L.-C. Chen, W.-W. Lin, J.-W. Chen, Fabrication of GaN-based white light-emitting diodes on yttrium aluminum garnet-polydimethylsiloxane flexible substrates, Ann. Mater. Sci. Eng. (2015) 1–5, https://doi.org/10.1155/2015/537163, 2015.
[28] D.E. Kuznetsova, G.A. Dosovitskiy, A.E. Dosovitskiy, Transparency and microstructure of YAG:Ce phosphor particles, Opt. Mater. (Amst). 66 (2017) 547–551, https://doi.org/10.1016/j.optmat.2017.02.042.
[29] E. Gordienko, A. Fedorov, E. Radiuk, V. Mechinsky, G. Dosovitskiy, E. Vashchenkova, D. Kuznetsova, V. Retivov, A. Dosovitskiy, M. Korjik, R. Sandu, Synthesis of crystalline Ce-activated garnet phosphor powders and technique to characterize their scintillation light yield, Opt. Mater. (Amst). 78 (2018) 312–318, https://doi.org/10.1016/j.optmat.2018.02.045.
[30] H. Cai, Y. Jiang, J. Feng, S. Zhang, F. Peng, Y. Xiao, L. Li, J. Feng, Preparation of silica aerogels with high temperature resistance and low thermal conductivity by monodispersed silica sol, Mater. Des. 191 (2020), 108640, https://doi.org/10.1016/j.matdes.2020.108640.
[31] P.B. Wagh, G.M. Pajonk, D. Haranath, A.V. Rao, Influence of temperature on the physical properties of citric acid catalyze TEOS silica aerogels, Mater. Chem. Phys. 50 (1997) 76–81, https://doi.org/10.1016/S0254-0584(97)80187-3.
[32] Y.-C. Lin, M. Karlsson, M. Bettinelli, Inorganic phosphor materials for lighting, Top. Curr. Chem. 374 (2016) 21, https://doi.org/10.1007/s41061-016-0023-5.
[33] D.A. Pardo, G.E. Jabbour, N. Peyghambarian, Application of screen printing in the fabrication of organic light-emitting devices, Adv. Mater. 12 (2000) 1249–1252, https://doi.org/10.1002/1521-4095(200009)12:17<1249::AID-ADMA1249>3.0.CO;2-Y.
[34] M. Brinkmann, G. Gadret, M. Muccini, C. Taliani, N. Masciocchi, A. Sironi, Correlation between molecular packing and optical properties in different crystalline polymorphs and amorphous thin films of mer -Tris(8-hydroxyquinoline) aluminum(III), J. Am. Chem. Soc. 122 (2000) 5147–5157, https://doi.org/10.1021/ja993608k.
[35] L. Klein, M. Aparicio, A. Jitianu (Eds.), Handbook of Sol-Gel Science and Technology, Springer International Publishing, Cham, 2018, https://doi.org/10.1007/978-3-319-32101-1.

[36] A.E. Lebedev, A.M. Katalevich, N.V. Menshutina, Modeling and scale-up of supercritical fluid processes. Part I: supercritical drying, J. Supercrit. Fluids 106 (2015) 122–132, https://doi.org/10.1016/j.supflu.2015.06.010.
[37] M. Thommes, K. Kaneko, A.V. Neimark, J.P. Olivier, F. Rodriguez-Reinoso, J. Rouquerol, K.S.W. Sing, Physisorption of gases, with special reference to the evaluation of surface area and pore size distribution (IUPAC Technical Report), Pure Appl. Chem. 87 (2015) 1051–1069, https://doi.org/10.1515/pac-2014-1117.
[38] R.I. Avetisov, A.A. Akkuzina, A.G. Cherednichenko, A.V. Khomyakov, I.C. Avetissov, Polymorphism of tris(8-hydroxyquinoline) aluminum, gallium, and indium, Dokl. Chem. 454 (2014) 6–8, https://doi.org/10.1134/S0012500814010029.
[39] I. Hernández, W.P. Gillin, Influence of high hydrostatic pressure on Alq 3 , Gaq 3 , and Inq 3 (q = 8-hydroxyquinoline), J. Phys. Chem. B 113 (2009) 14079–14086, https://doi.org/10.1021/jp905108x.
[40] O.B. Petrova, R.I. Avetisov, I.K. Avetisov, O.A. Mushkalo, A.V. Khomyakov, A.G. Cherednichenko, Hybrid materials based on organic luminophores in inorganic glass matrix, Opt Spectrosc. 114 (2013) 886–889, https://doi.org/10.1134/S0030400X13060131.
[41] O.B. Petrova, K.I. Runina, M.N. Mayakova, I.V. Taydakov, A.V. Khomyakov, R.I. Avetisov, I.C. Avetissov, Luminescent hybrid materials based on metal-organic phosphors in PbF2 powder and PbF2-containing glass matrix, Opt. Mater. (Amst). 88 (2019) 378–384, https://doi.org/10.1016/j.optmat.2018.11.055.
[42] M. Rajeswaran, T.N. Blanton, C.W. Tang, W.C. Lenhart, S.C. Switalski, D.J. Giesen, B.J. Antalek, T.D. Pawlik, D.Y. Kondakov, N. Zumbulyadis, R.H. Young, Structural, thermal, and spectral characterization of the different crystalline forms of Alq3, tris(quinolin-8-olato)aluminum(III), an electroluminescent material in OLED technology, Polyhedron 28 (2009) 835–843, https://doi.org/10.1016/j.poly.2008.12.022.